HOKKAIDO UNIVERSITY

Title	In situ/operando spectroscopic studies on NH3-SCR reactions catalyzed by a phosphorus-modified Cu-CHA zeolite
Author(s)	Kubota, Hiroe; Liu, Chong; Amada, Takehiro et al.
Citation	Catalysis today, 376, 73-80 https://doi.org/10.1016/j.cattod.2020.07.084
Issue Date	2021-09-15
Doc URL	https://hdl.handle.net/2115/90385
Rights	© 2021. This manuscript version is made available under the CC-BY-NC-ND 4.0 license http://creativecommons.org/licenses/by-nc-nd/4.0/
Rights(URL)	https://creativecommons.org/licenses/by-nc-nd/4.0/
Type	journal article
File Information	text_NH3-SCR_Cu-PCHA_2nd rev_2.pdf

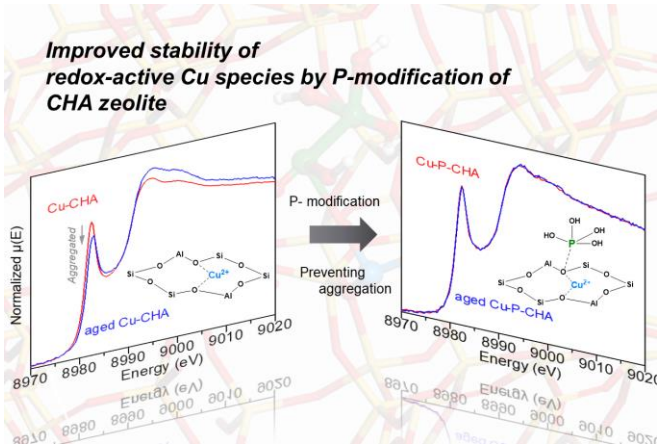
Hokkaido University Collection of Scholarly and Academic Papers : HUSCAP

In situ/operando spectroscopic studies on NH_3–SCR reactions catalyzed by a phosphorus-modified Cu-CHA zeolite

Hiroe Kubota,[a] Chong Liu,[a] Takehiro Amada,[a] Kenichi Kon,[a] Takashi Toyao,[a,b] Zen Maeno,[a] Kakuya Ueda,[c] Atsushi Satsuma,[b,c] Nao Tsunoji,[d] Tsuneji Sano,[d] Ken-ichi Shimizu*[a,b]

[a] Institute for Catalysis, Hokkaido University, N-21, W-10, Sapporo 001-0021, Japan
[b] Elements Strategy Initiative for Catalysts and Batteries, Kyoto University, Katsura, Kyoto 615-8520, Japan
[c] Department of Materials Chemistry, Graduate School of Engineering, Nagoya University, Furo-cho, Chikusa-ku, Nagoya, 464-8603, Japan
[d] Department of Applied Chemistry, Graduate School of Engineering, Hiroshima University, Higashi-Hiroshima 739-8527, Japan

Graphical abstract



Highlights

- *In situ/operando* spectroscopic investigations revealed the mechanism of the NH_3–SCR reaction over a heterogeneous Cu-exchanged phosphorus-modified CHA zeolite catalysts (Cu-P-CHA).
- The NH_3–SCR reaction over the Cu-P-CHA catalyst proceeds via the reduction of Cu(II) to Cu(I) and a subsequent re-oxidation of Cu(I) to Cu(II) similar to the system of Cu-exchanged CHA zeolite catalysts (Cu-CHA) without phosphorus modification.
- The phosphorus modification prevents the deactivation of the active Cu species in Cu-P-CHA during hydrothermal treatment.

Abstract

The modification of Cu-exchanged zeolites with phosphorus represents a promising method to enhance their hydrothermal stability, which is of pivotal importance for catalysts that promote the selective catalytic reduction of NO with ammonia (NH_3–SCR). In this study, we investigated the reaction mechanism of NH_3–SCR catalyzed by a phosphorus-modified CHA zeolite that contains active Cu species (Cu-P-CHA), and assessed the effect of the phosphorus modification on the hydrothermal stability of the catalyst by employing *in situ/operando* spectroscopic methods. In their entirety, the combined results from *in situ/operando* IR, UV-vis and XANES experiments revealed that the NH_3–SCR process over Cu-P-CHA proceeds via the reduction of Cu(II) to Cu(I) followed by a reoxidation of Cu(I) to Cu(II). In addition, we found that the phosphorus modification improved the hydrothermal durability of the catalyst by retaining a higher amount of the redox-active Cu species and the zeolite framework.

1 Introduction

The selective catalytic reduction of nitrogen oxides (NO_x) with ammonia (NH_3–SCR) for the control of diesel emissions is currently one of the hottest topics in environmental catalysis [1–4]. Various catalysts have been studied, and Cu-exchanged small-pore zeolites, such as CHA, AEI, RTH, and AFX, have attracted particular attention [5–11]. The Cu-exchanged CHA type SSZ-13 zeolite (Cu-CHA) is regarded to be the most suitable catalyst owing to its high activity and hydrothermal durability, which makes it practicably viable [12–19]. When Cu-CHA is used for NO_x emission control during diesel combustion, it is exposed to harsh conditions, and the strong demand to improve the catalyst stability given its vital importance in this real-world application is accordingly very high [20]. Two major degradation processes for such Cu-zeolite catalyst systems, have been identified: sulfur poisoning and hydrothermal aging [16,20–22]. The former is typically reversible because adsorbed sulfur species (mainly sulfate) can be removed by active regeneration treatments at high temperature [21]. The latter, however, is typically irreversible due to the permanent structural changes to the zeolite frameworks and owing to the changes to the chemical and/or physical nature of the active Cu species [20]. Improvement of the hydrothermal durability of catalyst systems is therefore of paramount importance for the design and manufacturing of advanced Cu-zeolite catalysts.

Recently, the group of Tsunoji and Sano have prepared phosphorus(P)-modified small-pore zeolites, including CHA, LEV, and AEI, as durable host materials in Cu-catalyzed NH_3–SCR reactions [23–25]. Although P-modification can improve the hydrothermal stability of zeolites [26–30], the typical procedure for carrying out this post-synthesis modification cannot be applied to small-pore zeolites as the diffusion of phosphorus species inside the small pores of the zeolite is limited. However, Tsunoji, Sano, and coworkers have achieved such P-modification by synthesizing P-modified zeolites from zeolitic starting materials. This process involves the hydrothermal conversion of the starting zeolite using a phosphonium-containing organic structure-directing agent (P-OSDA). This method

provides highly crystalline P-modified zeolites (P-zeolites) without structure-defects and with a homogeneous distribution of the P species inside the cavity [31]. Cu-loaded P-zeolites (Cu-P-zeolites) exhibit excellent catalytic performance with high thermal/hydrothermal stability in the NH_3–SCR process [24]. Although highly durable Cu-P-zeolite catalysts have been developed, the effect that the P species exerts on improving the catalyst stability and the SCR mechanism has not been studied systematically [25].

In the present study, the reaction mechanism of the standard NH_3–SCR reaction catalyzed by a Cu-loaded P-CHA zeolite catalyst (Cu-P-CHA) was investigated. For that purpose, various *in situ*/*operando* spectroscopic methods were employed, which revealed that the SCR reaction over the Cu-P-CHA catalyst proceeds by way of the reduction of Cu(II) to Cu(I), followed by a subsequent re-oxidation of Cu(I) to Cu(II), similar to Cu-CHA systems that have not been modified with phosphorous. Moreover, we discovered that the improved hydrothermal stability caused by the P-modification results from the suppression of the formation of aggregated Cu oxides (CuO_x), which are not redox-active during the NH_3–SCR process.

2 Experimental

Preparation of the Catalysts

An NH_4^+-type P-CHA zeolite (Si/Al = 10, P/Al = 0.18) and an NH_4^+-type CHA zeolite (Si/Al = 10) were synthesized according to a previously reported method [31]. It should be noted here that the P-CHA zeolite used in this study has an almost optimal P/Al ratio, as determined in a previous study of some of our authors [24]. The Si/Al ratio was determined by inductively coupled plasma-atomic emission spectroscopy (ICP-AES) on a Seiko SPS7000. To synthesize the Cu-P-CHA catalyst, dealuminated FAU zeolite (Si/Al = 16), sodium hydroxide, tetraethyl phosphonium hydroxide (TEP), *N*,*N*,*N*-trimethyl-1-adamantammonium hydroxide (TMAda), and distilled water were mixed to obtain a gel with a molar composition of Si/Al/TMAda/TEP/NaOH/H_2O = 1:0.0625:0.05:0.25:0.1:7.5. The resulting gel was transferred into a 100 mL Teflon-lined stainless-steel autoclave (R-100, Hiro Company) and heated to 150 °C for seven days with tumbling (10 rpm). The solid product was collected via centrifugation, washed thoroughly with distilled water until the washings exhibited an almost neutral pH, and then dried overnight at 70 °C. The as-synthesized zeolites were calcined for 10 h at 600 °C in air to remove organic molecules. The Na cations in the calcined zeolites were subsequently removed by ion-exchange using an aqueous solution of NH_4NO_3 (*ca.* 1.0 mol L^{-1}) at 60 °C for 2 h (this ion-exchange procedure was repeated three times). The Cu-P-CHA catalyst was prepared using an aqueous-phase Cu-ion-exchange method on the NH_4^+-type P-CHA zeolite using a $Cu(NO_3)_2$ solution at pH = 5.5. After the exchange, the sample was filtered, washed with distilled water, and dried for 12 h at 110 °C, followed by calcination for 1 h at 600 °C.

The Cu-CHA catalyst without P-modification was prepared in the same way as the Cu-P-CHA catalyst using FAU (Si/Al = 16) and omitting the TEP. The synthesis gel with a molar composition Si/Al/TMAda/NaOH/H_2O = 1:0.0625:0.30:0.1:7.5 was used. X-ray fluorescence spectroscopy revealed Cu loadings of 2.0 (Cu/Al = 0.26) and 2.0 (Cu/Al = 0.26) wt% for Cu-P-CHA and Cu-CHA, respectively. Aged Cu-P-CHA and Cu-CHA were prepared by treating the samples for 15 h at 800 °C under a flow of 3% H_2O/air (30 mL min^{-1}).

In situ/operando X-ray absorption spectroscopy (XAS)

Cu K-edge XAS measurements were performed in transmission mode using beamline BL-14B2 at SPring-8. A Si(111) single crystal was used to obtain a monochromatic X-ray beam. A self-supported wafer-form of the sample (diameter: *ca.* 7 mm) was placed in a quartz *in situ* cell under a 10% flow of O_2 diluted with He (1000 mL min^{-1}). A mass spectrometer (BELMass, MicrotracBEL Corp.) was used for analyzing the effluent gas. Normalization and linear combination fitting (LCF) analysis of the X-ray absorption near edge structure (XANES) were carried out using the Athena software package [32]. XANES spectra for the reference compounds, which were collected using equivalent data collection procedures with specific acquisition parameters optimized for each sample, were taken from our previous study [33]. They were either measured after *in situ* treatment of Cu-P-CHA or Cu-CHA, to

obtain a reference for Z-[Cu^{2+}] (Z = zeolite framework), or prepared as solution-phase complexes, namely $[Cu(NH_3)_4]^{2+}$ and $[Cu(NH_3)_2]^{+}$, according to literature procedures [34,35].

***In situ/operando* UV-vis spectroscopy**

Diffuse reflectance UV-vis measurements were performed at 200 °C using JASCO V-670. The light source was directed at the center of an integrating sphere through an optical fiber. The reflectance was converted into pseudo-absorbance using the Kubelka-Munk function. $BaSO_4$ was used to obtain a background spectrum. Gas mixtures were fed into a Cu-P-CHA sample (6.5 mg) at a flow rate of 100 mL min^{-1}. The relative concentration of N_2 in the outlet gas mixture was monitored using the same mass spectrometry apparatus used for the XAS measurements. The product concentration was quantified by calibrating the mass response.

***In situ/operando* IR spectroscopy**

IR spectra were recorded on a JASCO FT/IR-4600. Samples were pressed into a 40 mg self-supporting wafer and mounted in a quartz IR cell with CaF_2 windows. Spectra were measured by accumulating 20 scans at a resolution of 4 cm^{-1}. A reference spectrum of the catalyst wafer in He taken at the measurement temperature was subtracted from each spectrum. The mass spectrometry apparatus used for the UV-vis measurements was also used here.

Catalytic reactions

The standard NH_3–SCR (NO + NH_3 + O_2) reaction was performed in a fixed-bed flow reactor using 10 mg of the Cu-P-CHA catalyst and a flow rate of 100 mL min^{-1}. The composition of the feed gas was NO/NH_3/O_2/He = 500 ppm/500 ppm/10%/balance. The effluent gas was analyzed by IR spectroscopy and gas chromatography with a thermal conductivity detector (GC-TCD) (Agilent 490 micro-GC). It should be noted here that the presence of N_2O was not detected.

Other characterization technique

Powder X-ray diffraction (XRD) measurements were carried out using a Rigaku MiniFlex II/AP diffractometer with Cu-Kα radiation. Electron spin resonance (ESR) spectra were measured on a Bruker Biospin EMX plus spectrometer. The catalyst powder (*ca.* 10 mg) was added to a 5 mm quartz tube, and subsequently, the sample tube was filled with N_2 to remove the O_2. Spectra were measured at −173 °C without exposure to air. N_2 adsorption measurements at −196 °C were carried out using an AUTOSORB 6AG (Yuasa Ionics Co.).

3. Results and discussion

3.1. Mechanistic investigation of the Steady-state standard NH_3–SCR

The oxidation state of the Cu species in the Cu-P-CHA was investigated under steady-state standard NH_3–SCR conditions by employing *in situ* Cu K-edge XANES techniques [8,33,36,37]. The low-contact time-conditions (W/F = 3.0×10^{-3} g s mL^{-1}; W = 50.6 mg; F = 1000 mL min^{-1}) allowed us to analyze the Cu oxidation states under kinetically controlled conditions. Fig. 1(a) shows the typical XANES spectra of Cu-P-CHA. By increasing the temperature from 150 °C to 400 °C, the peak characteristic of the Cu^+ species at 8983 eV increased. LCF analysis of the XANES spectra was performed on the spectra of the three reference compounds: $[Cu(NH_3)_4]^{2+}$ and $[Cu(NH_3)_2]^+$ in aqueous solution measured at room temperature, as well as the framework-interacting Z-$[Cu^{2+}]$ species [33]. A typical example of an LCF analysis is shown in Fig. 1(b); the *in situ* XANES spectrum obtained during the NH_3–SCR at 200 °C fits the combination of the aforementioned three reference spectra well. The error bars for the LCF analysis are given in Table S1. The temperature dependence of the fraction of each Cu species present is shown in Fig. 1(c). The fraction of the Cu(I) species $[Cu(NH_3)_2]^+$ is low at 150 °C and increases with increasing reaction temperature up to 300 °C. Yet, at high temperatures (>350 °C), the Z-$[Cu^{2+}]$ fraction surges substantially, which suggests a detachment of NH_3 from the Cu center.

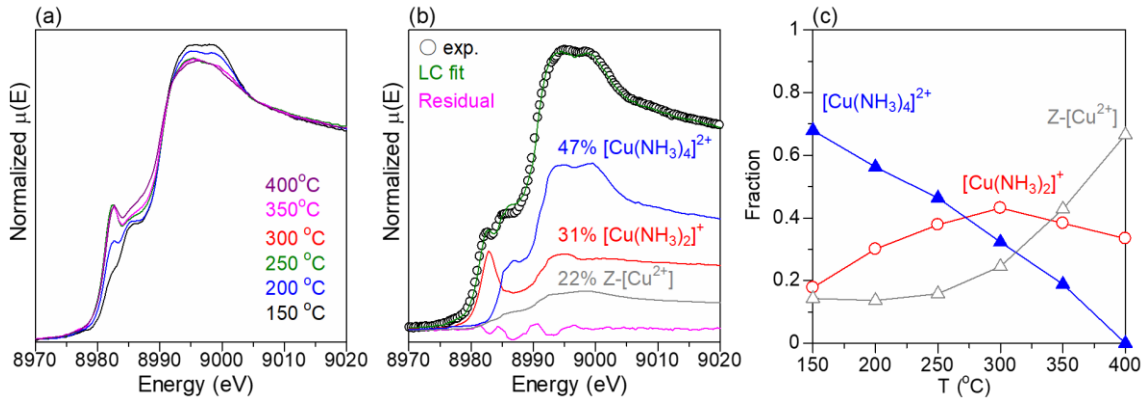


Fig. 1 *In situ* Cu K-edge XANES spectra of (a) Cu-P-CHA under NH_3–SCR reaction conditions at various temperatures. (b) LCF analysis of the Cu-P-CHA spectrum at 200 °C using the spectra of standard compounds. (c) Proportion of each Cu species present at different reaction temperatures when using the Cu-P-CHA catalyst. NH_3–SCR reaction conditions: 1000 ppm NH_3, 1000 ppm NO, 10% O_2, He balance (1000 mL min^{-1}); catalyst weight = 50.6 mg.

Operando UV-vis spectra of Cu-P-CHA during NH_3–SCR at 200 °C obtained using varying O_2 pressures (0–10%) are shown in Fig. 2(a). The spectra show a distinct band at around 760 nm due to d-d transitions in the Cu(II) species [36]. The intensity of the band at 760 nm was plotted as a function of the O_2 pressure together with the mass spectrum (MS) intensity of N_2 as shown in Fig. 2(b). Initially, the rate of the NH_3–SCR and the relative amount of Cu(II) species present increase steeply as the O_2

Cu(II)limiting step of NH_3–SCR at low O_2 concentration conditions, which can occur during the real-world operation of diesel vehicles, in particular during rapid acceleration.

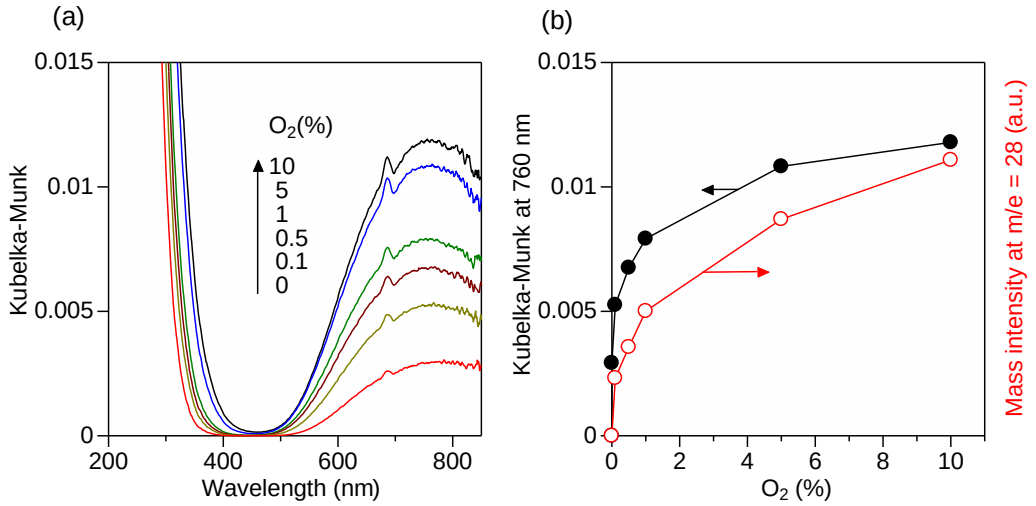


Fig. 2 (a) *Operando* UV-vis spectra of Cu-P-CHA during the NH_3–SCR at 200 °C using varying O_2 pressures (0.1-10%). (b) Black line - band intensity at 760 nm due to d–d transitions in Cu(II) during the NH_3–SCR as a function of the O_2 pressure. Red line - MS intensity of N_2 as a function of the O_2 pressure. Conditions: 1000 ppm NH_3, 1000 ppm NO, 10% O_2, He balance (100 mL min^{-1}); sample weight = 10 mg.

3.2. Mechanistic investigation of the reduction half-cycle

Operando XANES measurements were carried out to investigate the reduction half-cycle via the reaction of O_2-treated Cu-P-CHA with a mixture of NO and NH_3 (NO + NH_3) at 200 °C. The XANES spectrum of Cu-P-CHA after treatment with 10% O_2 treatment is shown in Fig. 3(a). Characteristic shoulders and peaks of isolated Cu^{2+} coordinated to the cation-exchange sites of the zeolite were observed from 8970 to 9020 eV [35,38–40]. After exposure of the sample to NO + NH_3, a sharp peak, which was attributed to the 1s → 4p transitions of the linear $[Cu(NH_3)_2]^+$ species, emerges at *ca.* 8980 eV [35,38,41]. During the reaction, the formation of N_2 was confirmed by mass spectrometry. The formation of $[Cu(NH_3)_2]^+$ and N_2 during the reduction half-cycle is consistent with previously reported results [33].

To obtain further insight into the mechanism of the reduction half-cycle of the NH_3–SCR, *operando* IR measurements were conducted for the reaction of the adsorbed NH_3 species with NO at 200 °C (Fig. 4). An IR spectrum was taken after feeding 0.1% NH_3 to Cu-P-CHA, followed by purging with He. The spectrum (Fig. 4(a), black line) shows a peak at 1620 cm^{-1} due to the coordination of NH_3 to Cu sites (Cu^{n+}-NH_3) and a large peak at 1430 cm^{-1} due to the presence of NH_4^+ (NH_3 on Brønsted acid sites) [42–44]. Subsequently, NO (500 ppm) was fed to the sample and the resulting Cu^{n+}-NH_3 band at 1620 cm^{-1} is shown by the red line in Fig. 4(a) red line. Fig. 4(b) shows the time-dependent MS intensity of N_2 downstream from the IR cell. The formation of N_2 coincides with the consumption of NH_3 on Cu, which indicates that the NH_3 at the Cu sites reacts with NO to yield N_2. NH_4^+ could be consumed under NO+O_2 [45,46]. We have recently reported that NH_4^+ in a Cu-zeolite does not react with NO at 200 °C in the absence of O_2 [33]. Based on the various aspects of spectroscopic evidence, we have shown that the reaction of Cu(II)-NH_3 with NO yields H^+, N_2, and H_2O [33]. The reaction of the thus formed H^+ with an adsorbed molecule of NH_3 could hence increase the amount of NH_4^+. As shown in Fig. 4, the intensity of the band due to NH_4^+ (1430 cm^{-1}) is increased by the reduction of the Cu(II)-NH_3 species with NO. This is consistent with a report by Simon et al. where the amount of NH_4^+ increases upon treating the Cu(II)-NH_3 species with NO [47].

Operando UV-vis measurements were carried out (Fig. 5). The UV-vis spectra for NH_3 adsorbed on Cu-P-CHA exhibits a d-d band centered around 760 nm that results from the Cu^{2+} species coordinated to a NH_3-ligand, which is consistent with the results obtained from the *operando* IR studies (Fig. 4). After purging with He and the subsequent introduction of NO, the d-d band almost disappeared, which is indicative of the reduction of Cu(II) to Cu(I). The formation of N_2 was also observed during the UV-vis measurements.

To check that the above reduction half-cycle is the main pathway for the formation of N_2 during the NH_3–SCR reaction, we compared the N_2 formation rate for the transient and steady-state NH_3–SCR reactions. The solid line in Fig. 6 shows the formation rate of N_2 during the transient reaction of the adsorbed NH_3 species with NO at 150 °C. This data was obtained using a conventional flow reactor

equipped with an online GC-TCD. The powder form of Cu-P-CHA was first exposed to 0.1% NH_3, followed by purging with He. As NO (500 ppm) was fed to the catalyst, the transient formation of N_2 was observed. The N_2-formation rate in the steady-state NH_3–SCR at 150 °C with the same reactor (in Fig. 6 dashed line) was of the same order of magnitude. The obtained result demonstrates that the reduction half-cycle is the most important N_2-formation step in the Cu-P-CHA-catalyzed NH_3–SCR at 150 °C. This finding is consistent with our previous report [33].

Summarizing the results of these three *operando* spectroscopic studies, it can be concluded that the reaction of the $[Cu(NH_3)_4]^{2+}$-like species with NO yields a $[Cu(NH_3)_2]^{+}$ species and N_2 in the gas phase. This mechanism is consistent with the previously reported mechanism of the Cu(II) → Cu(I) half-cycle for the NH_3-SCR catalyzed by Cu-CHA [48].

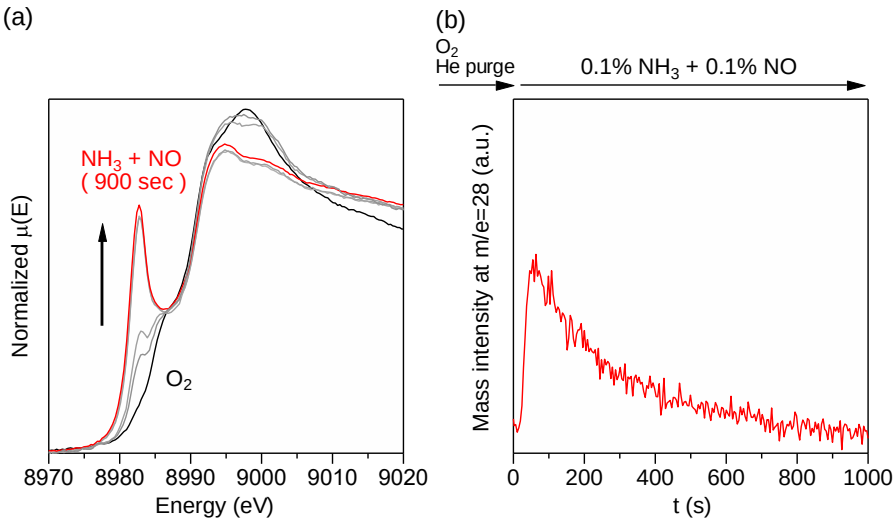


Fig. 3 (a) *Operando* XANES spectra of Cu-P-CHA obtained at 200 °C. The catalyst was first exposed to a flow of 0.1% NH_3/0.1% NO/He flow (1000 mL min^{-1}); (b) Time dependence of the MS intensity of N_2. Sample weight = 50.6 mg.

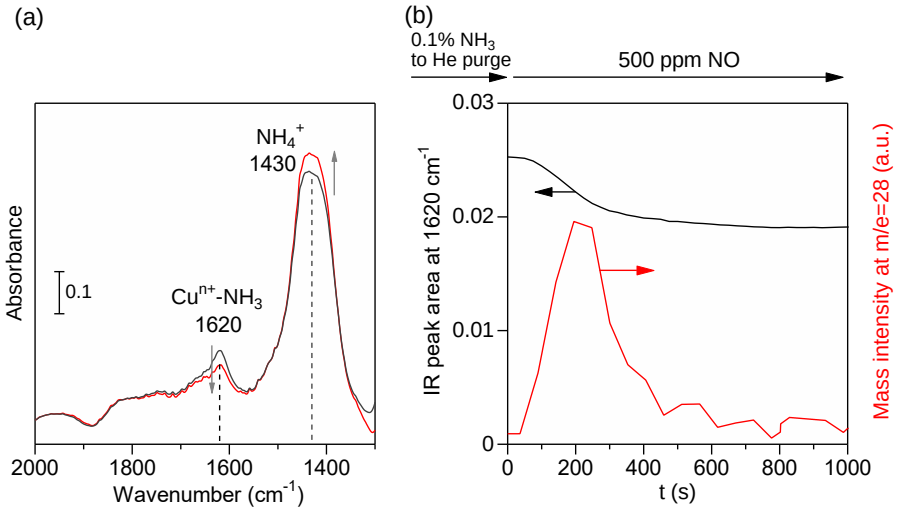


Fig. 4 (a) *Operando* IR spectra of adsorbed species in Cu-P-CHA obtained at 200 °C. The catalyst was first exposed for 0.5 h to a flow of 0.1% NH_3/He (100 mL min^{-1}) and purged for 10 min with He (black line), followed by exposure to a 500 ppm NO/He flow (100 mL min^{-1}; red line). (b) Time dependence

of the IR peak area due to adsorption of NH_3 on Cu sites (black line) and time dependence of the MS intensity of N_2 (red line). Sample weight = 40 mg.

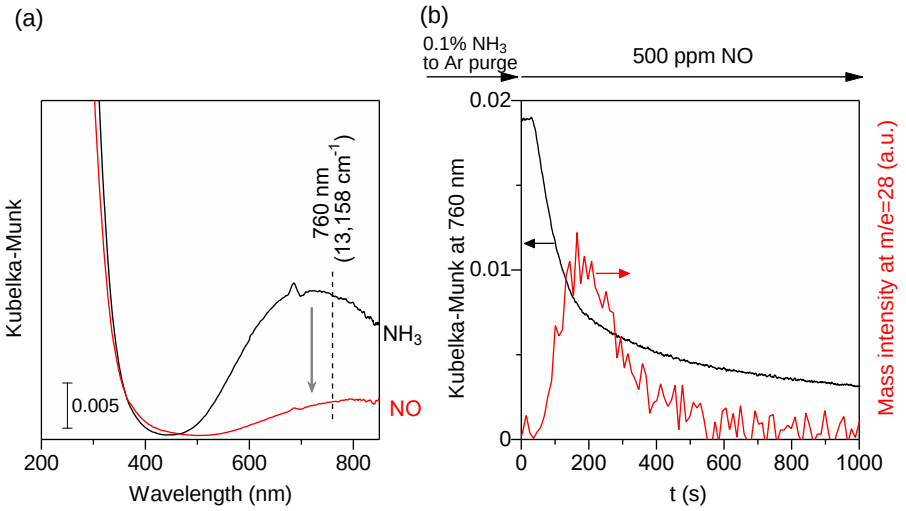


Fig. 5 (a) *Operando* UV-vis spectra of Cu-P-CHA obtained at 200°C. The catalyst was first oxidized under 10% O_2/He (100 mL min^{-1}), followed by exposure to a 0.1% NH_3/He flow (100 mL min^{-1}) for 0.5 h, and to a 500 ppm NO/He flow (100 mL min^{-1}). (b) Time dependence of the band intensity due to Cu(II) (black line) and time dependence of the MS intensity of N_2 (red line). Sample weight = 10 mg.

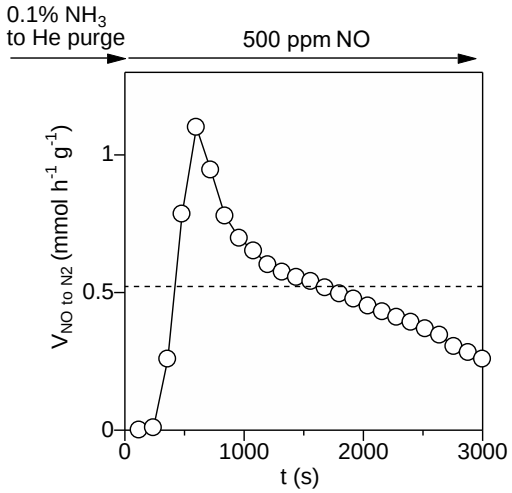


Fig. 6 Comparison of the steady-state (dashed line) and transient rates (solid line) of the NO reduction to N_2 over Cu-P-CHA at 150 °C. The steady-state rate was measured under the standard NH_3–SCR conditions. The transient reaction for the reduction half-cycle was carried out by passing 500 ppm NO/He (100 mL min^{-1}) over Cu-P-CHA pre-exposed to a 0.1% NH_3/He flow (0.5 h). Sample weight = 10 mg.

3.3. Mechanistic investigation of the oxidation half-cycle

In situ XANES measurements were also conducted for the oxidation half-cycle at 200 °C (Fig. 7). Recently, we discovered in a mechanistic study of the NH_3–SCR over Cu-CHA catalysts with the same Si/Al and Cu/Al ratios that the oxidation half-cycle can proceed using O_2 as the sole oxidant [33]. This has also been confirmed using a theoretical approach based on density functional theory (DFT) calculations [49]. In this study, after the reduction of Cu-P-CHA with NH_3 + NO, the sample was treated with 10% O_2 to induce the oxidation of Cu(I). In the XANES spectrum, the decrease of the peak arising from Cu(I) confirms the occurrence of oxidation. An LCF analysis was conducted for each spectrum to estimate the fraction of Cu(I) and Cu(II) present. The time dependence of the fraction of Cu(I) and Cu(II) is shown in Fig. 7(b). The fraction of Cu(II) increased immediately and then leveled off after 500 s. The time-dependency of the fractions of the Cu(II) and Cu(I) species for Cu-P-CHA were similar to those for the Cu-CHA system with similar Si/Al and Cu/Al ratios described in our recent experimental study [33]. This result indicates that the re-oxidation of Cu(I) in the form of the $[Cu(NH_3)_2]^+$ complex proceeds smoothly using O_2 as the sole oxidant via formation of multinuclear Cu species [49,50].

The results of the *in situ* UV-vis measurements for the oxidation half-cycle are shown in Fig. 8. When the Cu-P-CHA catalyst, pre-reduced by NO/NH_3, had been exposed to 10% O_2, the peak at 760 nm due to the presence of the Cu(II) emerged. This result indicates that the re-oxidation of Cu(I) to Cu(II) occurs with O_2 as the sole oxidant. In addition, the rate of the oxidation process is almost identical to the one obtained over the Cu-CHA catalyst in the absence of any P species [33]. The combined results of these *in situ* spectroscopic measurements suggest that the re-oxidation of Cu(I) proceeds via the same mechanism for both the Cu-CHA and Cu-P-CHA catalysts, regardless of the presence/absence of the P species.

Based on the above experimental results and our recent theoretical study [49], it is feasible to propose the following reaction mechanism for the NH_3–SCR over Cu-P-CHA: In the reduction half cycle, Cu(II) species with NH_3 ligands are reduced by NO to yield Cu(I) species, H^+ (in the form of NH_4^+), N_2, and H_2O. The Cu(I) species can be oxidized using O_2 as a sole oxidant to yield the original NH_3-solvated Cu(II) species. The mechanism is essentially the same as the NH_3–SCR mechanism catalyzed by Cu-CHA [33]. It should be noted here that the reaction does not necessarily proceed via this proposed mechanism, as several other catalytic pathways, which depend on the local reaction environment and the reaction conditions, can be envisioned [50].

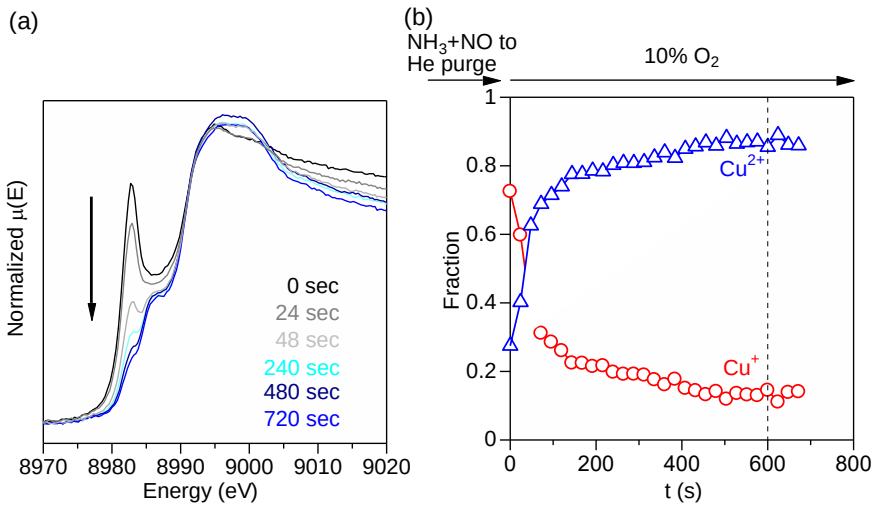


Fig. 7 (a) *In situ* XANES spectra of Cu-P-CHA, pre-reduced by NH_3/NO, during the re-oxidation half-cycle (under 10% O_2) at 200 °C. (b) Time-dependence of the fractions of Cu(II) and Cu(I) as estimated by *in situ* XANES spectra of Cu-P-CHA, pre-reduced by NH_3/NO, during the re-oxidation half cycle (under 10% O_2) at 200 °C. The catalyst was exposed to a 0.1% NH_3/0.1% NO/He flow (1000 mL min^{-1}) for 0.5 h, followed by exposure to 10% O_2/He (1000 mL min^{-1}) for 0.5 h after purging with He. Sample weight = 50.6 mg.

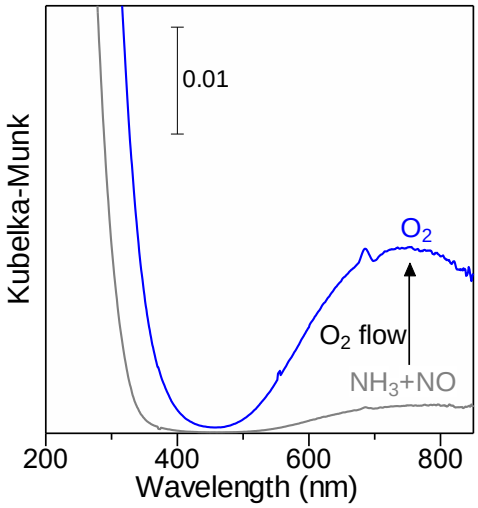


Fig. 8 *In situ* UV-vis spectra of Cu-P-CHA at 200 °C after reduction by NH_3/NO (gray line), followed by re-oxidation for 0.5 h under 10% O_2/He (blue line). The catalyst was exposed to a 0.1% NH_3/0.1% NO/He flow (100 mL min^{-1}) for 0.5 h, followed by exposure to 10% O_2/He (100 mL min^{-1}) for 0.5 h after purging with He; Sample weight = 10 mg.

3.4. Effect of P species on the catalyst stability

Improvement of the hydrothermal durability of NH_3–SCR catalysts is of great importance for real-world applications, and therefore, much effort has been devoted in recent years [51–53]. As mentioned in the introduction, Cu-P-CHA is very robust under hydrothermal conditions [31]. To investigate the effects of the presence of P species on the stability of Cu-P-CHA, XRD, XANES and ESR measurements were conducted on both fresh and aged catalysts samples. The aged catalysts samples were prepared using a hydrothermal method, where the samples were treated for 15 h at 800 °C under a flow of 3% H_2O/air. As shown in Fig. 9, the XRD patterns of the fresh and aged Cu-P-CHA are essentially identical, indicating that the zeolite framework of the Cu-P-CHA catalyst remained intact even after the hydrothermal treatment at 800 °C. In contrast, the diffraction peaks for the aged Cu-CHA shifted to higher angles compared to the fresh Cu-CHA, suggesting that the lattice parameter of the CHA zeolite decreased upon aging. Bayerlein et al. have reported the effect of hydrothermal dealumination on the lattice constant of FAU zeolites and shown that lattice parameter decreased with decreasing amounts of framework Al [54]. Accordingly, our XRD results for Cu-CHA suggest a dealumination of the CHA zeolite after the hydrothermal treatment at 800 °C, resulting in a decreased lattice parameter of the CHA zeolite. We also performed N_2 adsorption experiments of fresh and aged Cu-P-CHA. The BET specific surface areas were calculated to be 562 m^2/g and 591 m^2/g for fresh and aged samples, respectively, indicating that the porous zeolitic structure was maintained even after the aging treatment. These results clearly demonstrate that P-modification can improve the hydrothermal stability of Cu-CHA-type catalysts.

The nature of the Cu species after the hydrothermal treatment was investigated by *in situ* XANES measurements (Fig. 10). After exposing the samples to 10% O_2/He at 200 °C, the samples were reduced under a flow of NO/NH_3. For all samples, the spectra obtained after oxidation with O_2 were essentially identical and did not change whether there were P species present nor if the sample had undergone hydrothermal aging treatment at 800 °C. This result shows that the Cu species in these samples are Cu^{2+} species. After reduction by NO/NH_3, the XANES spectra of the fresh and aged Cu-P-CHA samples are similar and comparable to the reference spectrum of the $[Cu(NH_3)_2]^+$ complex (Fig. 1(b)). In contrast, the XANES spectrum of the NO/NH_3-reduced aged Cu-CHA catalyst shows a different shape compared to that of the fresh sample. The intensity of the peak due to the presence of the $[Cu(NH_3)_2]^+$ species was decreased by the hydrothermal treatment. This indicates that the amount of redox-active Cu species, most likely isolated Cu ions, is decreased by the hydrothermal treatment.

Subsequently, we investigated the effect of the hydrothermal aging on the Cu species by ESR spectroscopy. Cu^{2+} is a d^9 system with an unpaired electron, which affords a spin doublet ground state [36,55]. Moreover, it has been reported that Cu−O−Cu dimers, CuO_x clusters, and bulk CuO are ESR-silent even though Cu^{2+} is paramagnetic. The relative amounts of the isolated Cu^{2+} ions in the zeolite frameworks can thus be estimated using ESR techniques [20]. ESR spectra of the fresh and aged Cu-P-CHA and Cu-CHA samples were measured at –173 °C (Fig. 11). The ESR spectra of the fresh Cu-CHA

and Cu-P-CHA samples exhibit sharp signals with g values ($g_{\perp}$ = 2.09 and $g_{\parallel}$ = 2.39) that can be assigned to monomeric Cu^{2+} ions in the CHA zeolites [55]. The intensities of these signals for the aged samples decreased, indicating that the hydrothermal treatment causes the aggregation of isolated Cu^{2+} ions to yield ESR-silent CuO_x species [20]. However, in the case of aged Cu-P-CHA, the magnitude of the decrease was considerably smaller than that observed for Cu-CHA. These results indicate that aggregation of isolated Cu^{2+} ions into an ESR-silent CuO_x species was suppressed by the P-modification. Summarizing the results of the XRD, XANES and ESR measurements, it can be concluded that the P species in the Cu-P-CHA catalyst effectively hampers the formation of redox-inactive CuO_x aggregates and therefore prevents the deactivation of the redox-active Cu species (isolated Cu ions).

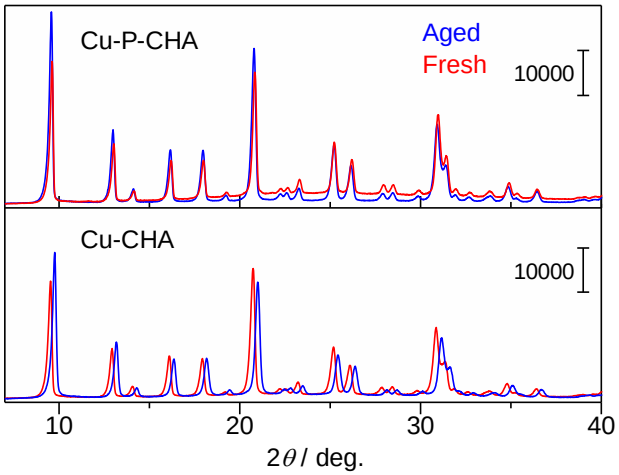


Fig. 9 XRD patterns of Cu-P-CHA and Cu-CHA before and after the hydrothermal treatment.

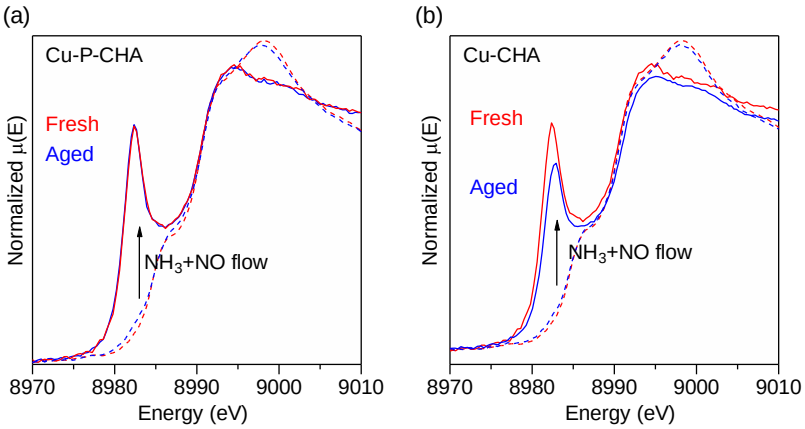


Fig. 10 *In situ* XANES spectra of (a) fresh Cu-P-CHA and aged Cu-P-CHA, (b) fresh Cu-CHA and aged Cu-CHA at 200 °C after initial oxidation under 10% O_2/He (1000 mL min^{-1}) (dashed line), followed by reduction under 0.1% NH_3/0.1% NO/He (1000 mL min^{-1}) (solid line); sample weight: 50.6 mg.

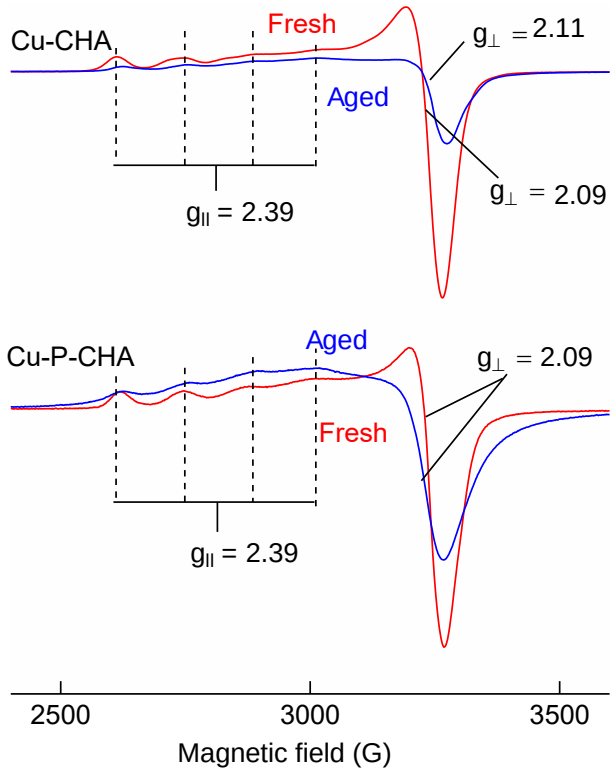


Fig. 11 ESR spectra of Cu-CHA and Cu-P-CHA before and after hydrothermal treatment.

4 Conclusions

This study investigated the redox cycle of the selective catalytic reduction of nitrogen oxides (NO_x) with ammonia (NH_3–SCR) catalyzed by a Cu-loaded phosphorous-modified CHA zeolite catalyst (Cu-P-CHA) using *in situ/operando* IR, UV-vis spectroscopy techniques as well as XAS measurements. Transient *operando* studies demonstrated that NH_3 adsorbed on Cu^{2+} as a Lewis acid site was consumed under a flow of NO to afford N_2 while Cu^{2+} was reduced to Cu^{+}. We also confirmed that the re-oxidation step of Cu^{+} was promoted by O_2 as the sole oxidant. In addition, the effects of the P species on the hydrothermal stability of the catalyst were also investigated. The obtained results demonstrated that the role of the P-modification is to suppress dealumination of the zeolite host and aggregation of active Cu^{2+} ions into redox-inactive CuO_x species during the hydrothermal treatment.

Acknowledgments
This research is promoted by the research association of Automotive Internal Combustion Engines (AICE) and financially supported by the Japanese Ministry of Economy, Trade and Industry and auto-industries. This work was also financially supported by the JST-CREST project JPMJCR17J3, KAKENHI grants 17H01341, 18K14057, and 18K14051 from the JSPS, as well as by the MEXT project "Elements Strategy Initiative to Form Core Research Centers (JPMXP0112101003) and the IRCCS. The authors sincerely thank the technical division of the Institute for Catalysis (Hokkaido University) for manufacturing the experimental equipment, and Prof. Hiroshi Hirata for his help with the ESR measurements. XAS measurements were performed at the BL-14B2 beamline of SPring-8 (JASRI; (proposal number 2019A1614). C.L. acknowledges the JSPS for a postdoctoral fellowship (P19059).

References

[1] A.M. Beale, F. Gao, I. Lezcano-Gonzalez, C.H.F. Peden, J. Szanyi, Chem. Soc. Rev. 44 (2015) 7371–7405.
[2] R. Zhang, N. Liu, Z. Lei, B. Chen, Chem. Rev. 116 (2016) 3658–3721.
[3] S.V. Priya, T. Ohnishi, Y. Shimada, Y. Kubota, T. Masuda, Y. Nakasaka, M. Matsukata, K. Itabashi, T. Okubo, T. Sano, N. Tsunoji, T. Yokoi, M. Ogura, Bull. Chem. Soc. Jpn. 91 (2018) 355–361.
[4] L. Han, S. Cai, M. Gao, J.Y. Hasegawa, P. Wang, J. Zhang, L. Shi, D. Zhang, Chem. Rev. 119 (2019) 10916–10976.
[5] D.W. Fickel, E. D'Addio, J.A. Lauterbach, R.F. Lobo, Appl. Catal. B Environ. 102 (2011) 441–448.
[6] T. Sonoda, T. Maruo, Y. Yamasaki, N. Tsunoji, Y. Takamitsu, M. Sadakane, T. Sano, J. Mater. Chem. A. 3 (2015) 857–865.
[7] N. Martín, C. Paris, P.N.R. Vennestrøm, J.R. Thøgersen, M. Moliner, A. Corma, Appl. Catal. B Environ. 217 (2017) 125–136.
[8] Y. Shan, X. Shi, J. Du, Y. Yu, H. He, Catal. Sci. Technol. 9 (2019) 106–115.
[9] G. Shibata, W. Eijima, R. Koiwai, K. Shimizu, Y. Nakasaka, Y. Kobashi, Y. Kubota, M. Ogura, J. Kusaka, Catal. Today. 332 (2019) 59–63.
[10] A. Chokkalingam, W. Chaikittisilp, K. Iyoki, S.H. Keoh, Y. Yanaba, T. Yoshikawa, T. Kusamoto, T. Okubo, T. Wakihara, RSC Adv. 9 (2019) 16790–16796.
[11] Y. Li, J. Deng, W. Song, J. Liu, Z. Zhao, M. Gao, Y. Wei, L. Zhao, J. Phys. Chem. C. 120 (2016) 14669–14680.
[12] J.H. Kwak, R.G. Tonkyn, D.H. Kim, J. Szanyi, C.H.F. Peden, J. Catal. 275 (2010) 187–190.
[13] J.S. McEwen, T. Anggara, W.F. Schneider, V.F. Kispersky, J.T. Miller, W.N. Delgass, F.H. Ribeiro, Catal. Today. 184 (2012) 129–144.
[14] Y. Xin, Q. Li, Z. Zhang, ChemCatChem. 10 (2018) 29 – 41.
[15] Y. Jangjou, Q. Do, Y. Gu, L.G. Lim, H. Sun, D. Wang, A. Kumar, J. Li, L.C. Grabow, W.S. Epling, ACS Catal. 8 (2018) 1325–1337.
[16] T. Usui, Z. Liu, S. Ibe, J. Zhu, C. Anand, H. Igarashi, N. Onaya, Y. Sasaki, Y. Shiramata, T. Kusamoto, T. Wakihara, ACS Catal. 8 (2018) 9165–9173.
[17] Y.J. Kim, P.S. Kim, C.H. Kim, Appl. Catal. A Gen. 569 (2019) 175–180.
[18] X. Auvray, A. Grant, B. Lundberg, L. Olsson, Catal. Sci. Technol. 9 (2019) 2152–2162.
[19] Y. Shan, X. Shi, G. He, K. Liu, Z. Yan, Y. Yu, H. He, J. Phys. Chem. C. 122 (2018) 25948−25953.
[20] J. Song, Y. Wang, E.D. Walter, N.M. Washton, D. Mei, L. Kovarik, M.H. Engelhard, S. Prodinger, Y. Wang, C.H.F. Peden, F. Gao, ACS Catal. 7 (2017) 8214–8227.
[21] J. Luo, D. Wang, A. Kumar, J. Li, K. Kamasamudram, N. Currier, A. Yezerets, Catal. Today. 267 (2016) 3–9.
[22] T. Ryu, N.H. Ahn, S. Seo, J. Cho, H. Kim, D. Jo, G.T. Park, P.S. Kim, C.H. Kim, E.L. Bruce, P.A. Wright, I.S. Nam, S.B. Hong, Angew. Chem. Int. Ed. 56 (2017) 3256–3260.
[23] Y. Kakiuchi, Y. Yamasaki, N. Tsunoji, Y. Takamitsu, M. Sadakane, T. Sano, Chem. Lett. 45 (2016) 122–124.
[24] Y. Kakiuchi, T. Tanigawa, N. Tsunoji, Y. Takamitsu, M. Sadakane, T. Sano, Appl. Catal. A Gen. 575 (2019) 204–213.
[25] P. Zhao, B. Boekfa, T. Nishitoba, N. Tsunoji, T. Sano, T. Yokoi, M. Ogura, M. Ehara, Microporous Mesoporous Mater. 294 (2020) 109908-109919.
[26] T. Blasco, A. Corma, J. Martínez-Triguero, J. Catal. 237 (2006) 267–277.
[27] N. Xue, R. Olindo, J.A. Lercher, J. Phys. Chem. C. 114 (2010) 15763–15770.
[28] P. Li, W. Zhang, X. Han, X. Bao, Catal. Lett. 134 (2010) 124–130.
[29] H.E. Van Der Bij, L.R. Aramburo, B. Arstad, J.J. Dynes, J. Wang, B.M. Weckhuysen, ChemPhysChem. 15 (2014) 283–292.
[30] H. Zhao, Y. Zhao, M. Liu, X. Li, Y. Ma, X. Yong, H. Chen, Y. Li, Appl. Catal. B Environ. 252 (2019) 230–239.

[31] Y. Yamasaki, N. Tsunoji, Y. Takamitsu, M. Sadakane, T. Sano, Microporous Mesoporous Mater. 223 (2016) 129–139.
[32] B. Ravel, M. Newville, J. Synchrotron Radiat. 12 (2005) 537–541.
[33] C. Liu, H. Kubota, T. Amada, K. Kon, T. Toyao, Z. Maeno, K. Ueda, J. Ohyama, A. Satsuma, T. Tanigawa, N. Tsunoji, T. Sano, K. Shimizu, ChemCatChem. 12 (2020) 3050–3059.
[34] K.A. Lomachenko, E. Borfecchia, C. Negri, G. Berlier, C. Lamberti, P. Beato, H. Falsig, S. Bordiga, J. Am. Chem. Soc. 138 (2016) 12025–12028.
[35] T.V.W. Janssens, H. Falsig, L.F. Lundegaard, P.N.R. Vennestrøm, S.B. Rasmussen, P.G. Moses, F. Giordanino, E. Borfecchia, K.A. Lomachenko, C. Lamberti, S. Bordiga, A. Godiksen, S. Mossin, P. Beato, ACS Catal. 5 (2015) 2832–2845.
[36] A.R. Fahami, T. Günter, D.E. Doronkin, M. Casapu, D. Zengel, T.H. Vuong, M. Simon, F. Breher, A. V. Kucherov, A. Brückner, J.D. Grunwaldt, React. Chem. Eng. 4 (2019) 1000–1018.
[37] K. Ueda, J. Ohyama, A. Satsuma, Chem. Lett. 46 (2017) 1390–1392.
[38] C.W. Andersen, E. Borfecchia, M. Bremholm, M.R.V. Jørgensen, P.N.R. Vennestrøm, C. Lamberti, L.F. Lundegaard, B.B. Iversen, Angew. Chem. Int. Ed. 56 (2017) 10367–10372.
[39] B. Kerkeni, D. Berthout, D. Berthomieu, D.E. Doronkin, M. Casapu, J.D. Grunwaldt, C. Chizallet, J. Phys. Chem. C. 122 (2018) 16741–16755.
[40] A.G. Greenaway, I. Lezcano-Gonzalez, M. Agote-Aran, E.K. Gibson, Y. Odarchenko, A.M. Beale, Top. Catal. 61 (2018) 175–182.
[41] A. Marberger, A.W. Petrov, P. Steiger, M. Elsener, O. Kröcher, M. Nachtegaal, D. Ferri, Nat. Catal. 1 (2018) 221–227.
[42] H. Zhu, J.H. Kwak, C.H.F. Peden, J. Szanyi, Catal. Today. 205 (2013) 16–23.
[43] I. Lezcano-Gonzalez, U. Deka, B. Arstad, A. Van Yperen-De Deyne, K. Hemelsoet, M. Waroquier, V. Van Speybroeck, B.M. Weckhuysen, A.M. Beale, Phys. Chem. Chem. Phys. 16 (2014) 1639–1650.
[44] Y. Shan, X. Shi, J. Du, Y. Yu, H. He, Catal. Sci. Technol. 9 (2019) 106–115.
[45] D. Wang, Y. Peng, S. Xiong, B. Li, L. Gan, C. Lu, Appl. Catal. B Environ. 221 (2018) 556–564.
[46] S. Xiong, Y. Peng, D. Wang, N. Huang, Q. Zhang, S. Yang, J. Chen, J. Li, Chem. Eng. J. 387 (2020) 124090-124101.
[47] S.P. Chen, U. Simon, P. Chen, V. Rizzotto, U. Simon, React. Chem. Eng. 4 (2019) 986–994.
[48] C. Paolucci, A.A. Parekh, I. Khurana, J.R. Di Iorio, H. Li, J.D. Albarracin Caballero, A.J. Shih, T. Anggara, W.N. Delgass, J.T. Miller, F.H. Ribeiro, R. Gounder, W.F. Schneider, J. Am. Chem. Soc. 138 (2016) 6028–6048.
[49] C. Liu, H. Kubota, T. Toyao, Z. Maeno, K. Shimizu, Catal. Sci. Technol 12 (2020) 3586–3593.
[50] L. Chen, T. V. W. Janssens , P. N. R. Vennestrøm , J. Jansson , M. Skoglundh, H. Grönbeck, ACS Catal., 10 (2020) 5646–5656.
[51] J. Wang, H. Zhao, G. Haller, Y. Li, Appl. Catal. B Environ. 202 (2017) 346–354.
[52] H. Zhao, Y. Zhao, Y. Ma, X. Yong, M. Wei, H. Chen, C. Zhang, Y. Li, J. Catal. 377 (2019) 218–223.
[53] Y. Ma, H. Zhao, C. Zhang, Y. Zhao, H. Chen, Y. Li, Catal. Today. In press. doi:10.1016/j.cattod.2019.03.057.
[54] R. A. Beyerlein, G. B. McVicker, L. N. Yacullo, J. J. Ziemiak, J. Phys. Chem. 92 (1988) 1967–1970.
[55] A. Godiksen, P.N.R. Vennestrøm, S.B. Rasmussen, S. Mossin, Top. Catal. 60 (2017) 13–29.